Mechanical Systems and Signal Processing 163 (2022) 108149

Contents lists available at ScienceDirect

Mechanical Systems and Signal Processing

journal homepage: www.elsevier.com/locate/ymssp

Frequency attenuation band with low vibration transmission in a finite-size plate strip embedded with 2D acoustic black holes

Hongli Ji [a,1], Bing Han [a,1], Li Cheng [b], Daniel J. Inman [c], Jinhao Qiu [a,*]

[a] State Key Laboratory of Mechanics and Control of Mechanical Structures, Nanjing University of Aeronautics and Astronautics, 29 Yudao St, Nanjing 210016, China
[b] Department of Mechanical Engineering, Hong Kong Polytechnic University, Hung Hom, Kowloon 999077, Hong Kong
[c] Department of Aerospace Engineering, University of Michigan, 1320 Beal Ave, Ann Arbor, MI 48109, USA

ARTICLE INFO

Keywords:
Vibration attenuation band
Acoustic black hole
Local structural resonance
Modal transmission
Modal displacement cancellation

ABSTRACT

Acoustic Black Hole (ABH) structures allowing for wave manipulation and energy focalization have potential applications in broadband structural vibration suppression. In this work, the vibration transmission characteristics of a plate strip embedded with multiple two-dimensional (2D) ABH without additional damping material were investigated. Both the simulation and experimental results show that the investigated structure exhibits attenuation bands with low vibration transmission, and the vibration attenuation phenomenon appears in frequency ranges well below the cut-on frequency of the ABHs. The width and position of the attenuation bands depend on the number of ABHs. A numerical investigation was carried out on the mechanism of the attenuation band generation. The analysis results show dual physical effects: low modal transmission in asymmetrical structures and modal displacement cancellation on the receiving side in both asymmetrical and symmetrical structures. Strong local structural resonances induced by ABHs play an important role in modal transmission reduction, modal displacement cancellation and weak excitation of some modes. The attenuation phenomenon reveals a new ABH-specific feature which enriches the existing knowledge on ABH structures and broadens the design perspective of vibration attenuation through band creation.

1. Introduction

Capitalizing on the Acoustic Black Hole (ABH) phenomenon [1,2], innovative structures can be designed for various vibration control applications through manipulating the flexural wave propagation. Research on ABHs has been attracting a growing attention in the last decade due to their simple structural features and broadband wave focusing and energy dissipation characteristics [3–6]. The thickness of an ideal one-dimensional ABH structure is tailored according to a power-law-profile $h(x) = \varepsilon x^m$, $m \geq 2$, which results in the phase velocity of the flexural wave decreasing to zero as it approaches the tapered edge, and consequently leading to a theoretically zero wave reflection. Although an ideal ABH structure cannot be achieved because of the manufacturing limitations with unavoidable truncation at the wedge tip, flexural waves can still be effectively focalized and dissipated by properly tailoring the structural thickness and adopting suitable damping treatments, which is conducive to structural vibration suppression [3,7,8]. Analytical, numerical and

* Corresponding author.
E-mail address: qiu@nuaa.edu.cn (J. Qiu).
[1] These authors contributed equally to this work and should be considered co-first authors.

https://doi.org/10.1016/j.ymssp.2021.108149
Received 9 June 2020; Received in revised form 7 May 2021; Accepted 12 June 2021

experimental methods have been developed to investigate the damping characteristic of ABH structures [9–14]. It has been shown that systematic ABH phenomenon can be observed above the so-called characteristic frequency f_c (also called cut-on frequency) of the structure, defined as:

$$f_c = \frac{2\pi h}{D_{ABH}^2}\sqrt{\frac{E}{12\rho(1-\nu^2)}} \tag{1}$$

where D_{ABH} is the length of the ABH taper in one-dimensional case (1D) and the diameter of a 2D ABH indentation; h is the thickness of plate in the uniform area; E is the Young's modulus; ρ is the density [15,16]. At this frequency, the wavelength of the free bending wave is equal to the size of the ABH, so that $f_c \cdot D_{ABH}/c_0 = 1$ with c_0 being the phase velocity of flexural waves in the uniform area. Obviously, the application range of systems based on a single ABH cell is hampered below the cut-on frequency.

Attempts have been made to explore the use of multiple ABH cells in structures. In particular, the damping properties of a plate structure with a grid of ABHs have also been investigated [16,17]. Acoustic noise radiation of a plate can also be significantly suppressed by embedding multiple ABHs to impair its sound radiation efficiency [18,19]. A sandwich plate with embedded ABHs in the viscoelastic layer was also proposed to enhance the damping effect of ABH system at low frequency [20]. These studies bring focus on the vibration suppression caused by the effective energy dissipation of each individual ABH with a damping layer, but the possible wave manipulation characteristics caused by the interactions between multiple ABHs below the cut-on frequency of ABH cell were ignored. Interactions among ABHs have been investigated in a beam and a plate structure with an infinite lattice of one-dimensional (1D) ABHs [15,21–25]. These structures take the concept of phononic crystals with ABHs as the unit cells. The bandgap phenomenon was observed in the beam structure with one-dimensional ABH lattice and directional bandgaps were found in the plate structure with 1D ABH lattice. Indeed, a band structure analysis on infinite structures, focusing on the traveling wave propagation, is a useful approach to understand the bandgap phenomenon. Such an analysis also helps understand the energy attenuation characteristics of corresponding finite-size structures with sufficient periodic cells.

For engineering applications, designing proper ABH structures with acceptable mechanical properties is a challenge. One typical effort is the double-wall design, proposed in Ref. [26], to offer acceptable mechanical properties in terms of strength and stiffness of structure, while retaining typical ABH benefits. Along the same line of thinking, 2D ABHs can also offer better structural strength in a plate structure, in which 1D ABHs usually cut through the entire span-wide direction of the structure. The complications arising from such a design, however, are twofold: 1) the wave propagations in 2D ABHs are different from, and more complex than that in 1D ABHs [11,27]; and 2) additional energy transmission path through the uniform part of a plate is created. Moreover, perfect bandgaps which prohibit energy transmission exist in infinite lattice structures. Engineering applications, however, require the use of realistic structures, which are always finite in size, to achieve efficient energy isolation. It is therefore important to interrogate whether vibration attenuation could be achieved in a finite-size plate embedded with a finite number of 2D ABHs, especially when the number of ABH is not sufficient. If so, an appropriate analysis method should be established to fully understand the formation mechanism of such vibration attenuation phenomenon.

Motivated by this, this paper attempts to extend the application of ABH to vibration attenuation by investigating a plate strip embedded with multiple 2D ABHs. In this study, we consider a scenario in which only the inherent material damping is considered without additional damping materials over the structure to demonstrate the vibration phenomenon induced by the intrinsic properties of the ABH structure.

The outline of the paper is as follows. The finite-size plate strip with multiple ABHs without damping material is designed, followed by a description of the simulation model and experimental setup in Section 2. To facilitate performance evaluation, a uniform plate strip is selected as a benchmark case. The frequency band with low vibration transmission of the proposed structure, which is called the attenuation band, is then demonstrated through numerical simulation and experimental implementation in Section 3. The vibration attenuation phenomenon in the ABH plate can appear in frequency ranges well below the cut-on frequency of the ABH cell and the width and position of the attenuation bands depend on the number of ABHs, which is also observed by finite element method (FEM) simulations. Different from wave propagation analyses, steady state dynamics of the structure are analyzed to examine the final state of attenuation phenomena. The underlying physics is explored by scrutinizing structural modes and their contribution to the displacements on both the exciting side and receiving side in Section 4, which concludes that strong local structural resonance induced by ABH cells enriches vibration modes and induces reduction of modal transmission or cancellation of modal displacements. Finally, conclusions are drawn on the special vibration attenuation phenomenon and its mechanism of the proposed ABH structure in Section 5.

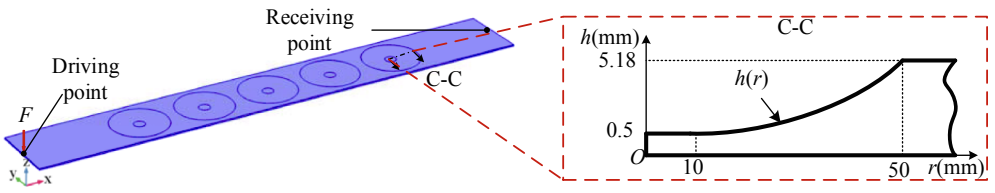

Fig. 1. Schematic of the finite-size plate strip and ABH thickness profile.

2. A finite-size plate strip with multiple ABHs and simulation model

2.1. Description of finite-size plate strip embedded with ABHs

The investigated structure is a thin plate strip embedded with multiple 2D ABHs, but without damping coating as shown in Fig. 1. Considering the limitation of machining precision and requirements of engineering applications, a modified 2D ABH profile indentation proposed by Huang et al. [27] was used. A uniform plate strip without ABHs was also investigated for comparison. Both the plate strip with ABHs and the uniform plate strip have the same dimensions of 0.8 m × 0.12 m with a thickness of 5.18 mm. As shown in Fig. 1, each ABH indentation consists of a tapered region and a plateau at its center. For the global coordinate system, the z-axis is in the thickness direction of the plate while the x-axis is along the length direction. Taking the center of ABH indentation as the origin of the local coordinate, the taper profile of the ABH indentation along the radial direction follows:

$$h(r) = \begin{cases} 0.5, (0 \leqslant r \leqslant 10) \\ 0.0029(r-10)^2 + 0.5, (10 \leqslant r \leqslant 50) \end{cases} (\text{mm}) \tag{2}$$

where r is the radial distance from the center of each ABH indentation. The schematic of spatial distribution of five ABH indentations is also illustrated in Fig. 2. The dash-dot lines denote the central position of each ABH indentation. In order to discuss the influence of ABH number and the distribution of ABH in the structure hereinafter, the number of ABHs is denoted by N, the distance between the position of the left excitation point and the center of the first ABH is defined as l_{c1}, and the distance between two adjacent ABHs is defined as l_d. In this study, all adjacent ABHs are equally spaced. The different placement of ABHs may destroy the symmetry of plate strip. The symmetric structure defined in this paper means that it has a symmetry axis perpendicular to the length direction of the plate strip. For example, five ABHs are uniformly distributed in a plate strip, which is a symmetric structure, as shown in Fig. 2.

Note the above 2D ABH strip offers higher stiffness than the corresponding 1D ABH counterpart [15], in which 1D ABH cuts through the entire width of the strip, but at the expense of creating additional energy transmission path through the uniform part of the strip. This direct energy transmission path, albeit narrow, makes the vibration isolation more challenging.

2.2. Experimental setup and FEM model

First, an experimental investigation is performed to reveal the phenomenon of vibration transmission in ABH-plates. For comparison, two types of elastic plates strip, one with five 2D ABH indentations (called ABH-plate) and the other without ABHs (called the uniform plate) were investigated. Both of them, made of aluminum and of the same size, were manufactured by computer numerical control (CNC) milling. The experimental setup is shown in Fig. 3. In order to achieve the free boundary conditions, the tested ABH-plate was suspended by four elastic strings. An electromagnetic shaker (B&K 4809), driven by a power amplifier (B&K 2718), was utilized to generate a periodic chirp signal from 10 Hz to 5000 Hz at a free end of the ABH-plate. A flexible slim rod was used to connect the shaker and the plate through a force transducer (PCB 208C02) to measure the excitation force. A Polytec Laser Scanning Vibrometer (PSV 500) was employed to scan the whole plate for response measurement.

FEM simulations were conducted to reveal the physical phenomenon on one hand, and to analyze the underlying physics of the attenuation band generation on the other hand. The solid mechanics interface in software COMSOL Multiphysis [28] is employed to develop 3D model and investigate the dynamics of plate strip by solving Navier's equations. The material properties used in the simulations are listed in Table 1. The loss factor η, which was used for consideration of inherent material damping, combines with the Young's modulus $\boldsymbol{E}$ to get a complex stiffness E^* [29]:

$$\boldsymbol{E}^* = (1 + j\eta)E \tag{3}$$

where j is the imaginary unit. Based on the three-dimensional equation of motion, all the models considered in this research were discretized by a quadratic Lagrange element. The considered frequency range is up to 5000 Hz. At least ten elements per local wavelength were ensured at the highest frequency in the simulation, so that the mesh in the tapered area is fine enough to guarantee the precision of analysis. Two layers of brick elements were arranged in the direction of the thickness to guarantee the calculation accuracy. All boundaries were set to be free. As shown in Fig. 1, a harmonic excitation force with a constant amplitude in the out-of-plane z direction was imposed at the midpoint on one free side of the panel.

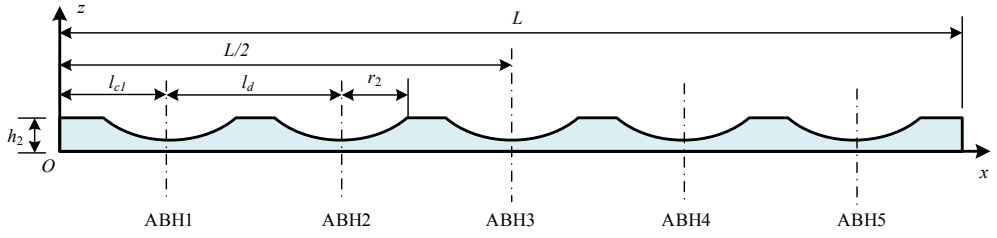

Fig. 2. Schematic plot showing the spatial distribution of ABHs in plate strip.

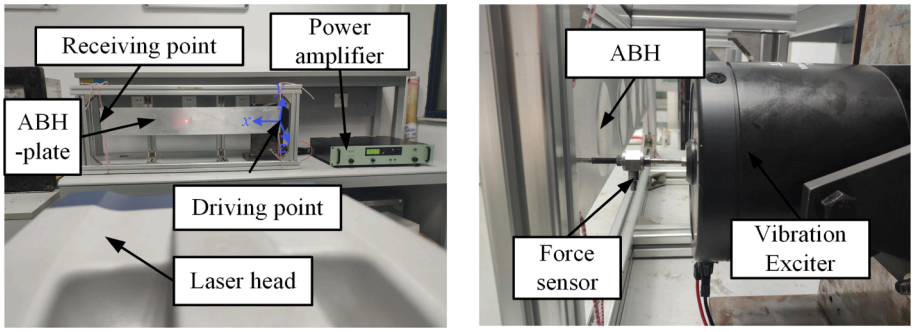

Fig. 3. Experimental set-up.

Table 1
Material parameters for FE model.

Plate strips	Mass density ρ(kg·m^{-3})	Young's modulus E(Pa)	Poisson's ratio ν	Loss factor η
	2820	7.1×10^{10}	0.33	1×10^{-3}

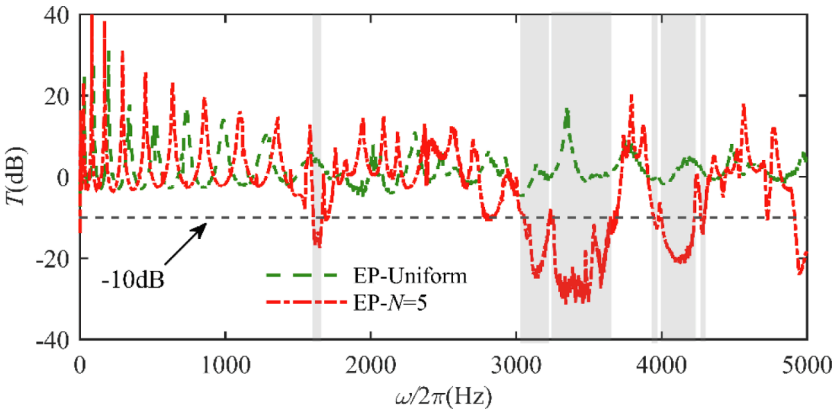

(a) Comparison of the transmission ratios T of ABH-plate and uniform plate

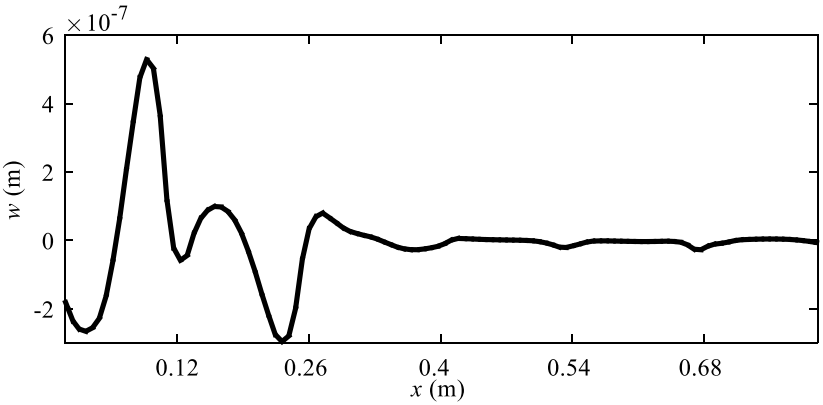

(b) Lateral displacement of ABH-plate along the centerline at 3550 Hz

Fig. 4. Experimental results of transmission ration and displacement of the ABH-plate.

3. ABH-induced vibration attenuation

The vibration attenuation property of the ABH-plate is quantified by the vibration transmission ratio defined as:

$$T = 20log\frac{\overline{w}_{out}}{\overline{w}_{in}} = 20log\frac{\frac{1}{M}\sum_{m=1}^{M}|\overline{w}(L,y_m)|}{\frac{1}{M}\sum_{m=1}^{M}|\overline{w}(0,y_m)|} \tag{4}$$

where $\overline{w}_{in}$ is the line-averaged flexural displacement amplitude on the excitation side of the plate strip (called driving side) and $\overline{w}_{out}$ is its counterpart on the receiving side; M represents the total number of points on the driving or receiving side used for averaging. Experiments were firstly conducted for an ABH-plate with $l_d = 0.14$ m and $l_{c1} = 0.12$ m to verify the vibration attenuation phenomenon. The vibration transmission ratio T of the ABH-plate with $N = 5$ as well as the uniform counterpart is presented in Fig. 4(a), in which the $T = 0$ means the equality of the averaged responses at both sides of the plate strip. The lateral displacement distribution of the ABH-plate along the centerline at the chosen frequency of 3550 Hz is also given in Fig. 4(b) to show the vibration attenuation pattern in the plate strip. As shown in the results, the vibration transmission of the ABH-plate is significantly reduced in three frequency bands around 1700 Hz, 3600 Hz as well as 4200 Hz, compared with the uniform plate. The frequency intervals corresponding to a transmission ratio lower than − 10 dB are therefore defined as the attenuation bands, marked as shaded regions in Fig. 4(a). Obviously, there exist attenuation bands in the ABH-plate, but not in the uniform plate. It should also be noted that the attenuation bands are well below the cut-on frequency of the ABH indentations, which, according to Eq. (1) and the parameters of Section 2.1, is 4990 Hz.

In order to further investigate the mechanism of the attenuation bands in the ABH-plate and the influence of different parameters on their formation, a numerical method based on FEM was used because it has the flexibility to change parameters systematically and to illustrate vibration modes. The experimental and numerical results of transmission ratio of both the ABH-plate and uniform plate are compared in Fig. 5 to verify the accuracy of the numerical model. Experimental results of the transmission ratio are in good agreement with numerical results except for the high frequencies, which indicates the existence of vibration attenuation bands. The noticeable deviation at high frequencies may be caused by a few factors: First, machining errors within the ABH cells, in terms of the thickness

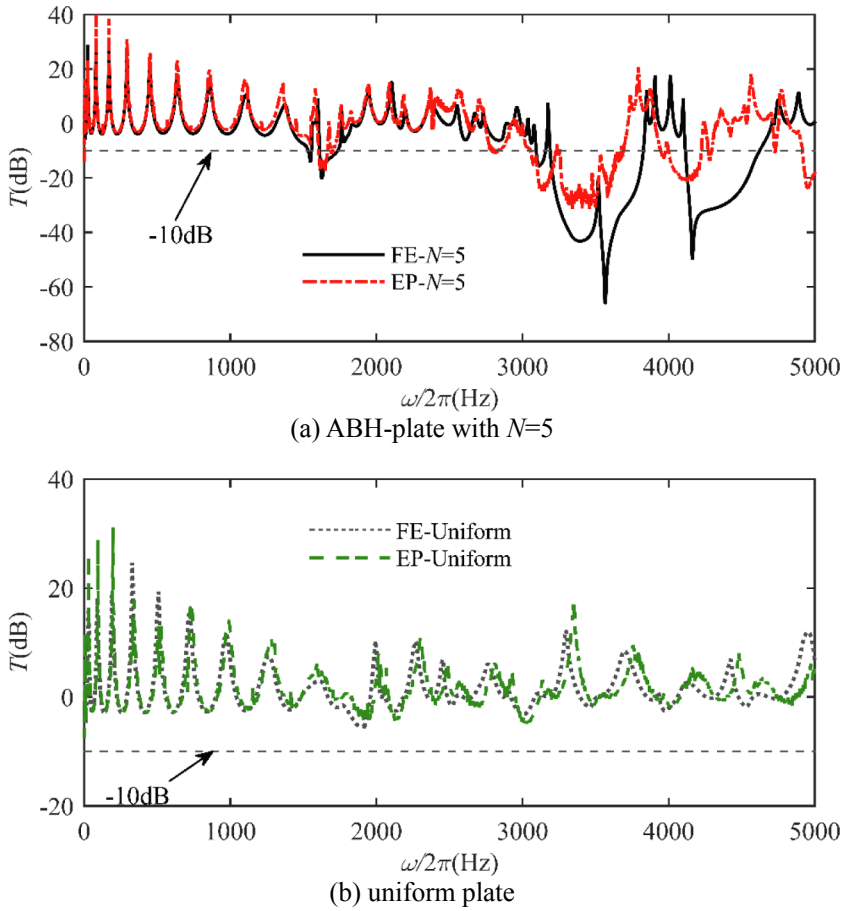

Fig. 5. Comparison between the experimental and simulation results of transmission ratio T.

profile and even surface irregularities, are inevitable. This would create discrepancies with the numerical model, especially for high-order modes, for which structural details play an increasingly important role. Second, even with small inconsistency in terms of damping parameters between the numerical model and experiment, the ABH-plate is more more sensitive to structural damping as compared with the uniform plate due to the large local strain and energy concentration in the former. Last, due to the weak vibration response of the structure, the influence of the measurement noise will become more obvious. Neverthless, experiments confirm typical phenomena predicted by the numerical simulations.

First, the influence of the number of ABH indentations on the attenuation bands is investigated numerically. The results of the vibration transmission ratio of three ABH-plates containing one, three and five ABHs ($N = 1, 3, 5$), respectively, are shown in Fig. 6 with vibration transmission ratio of the uniform plate as the reference. Two parameters l_d and l_{c1} in all three plate strips are the same as those used in the experiment. It can be seen that there are two narrow attenuation bands around 1700 Hz and 3600 Hz for the case $N = 1$. With the increasing number of ABHs in the plate strip, not only attenuation bands around 1700 Hz and 3600 Hz are broadened, but also a new attenuation band around 4300 Hz appears. Meanwhile, the attenuation effect is enhanced around 3600 Hz as the number of

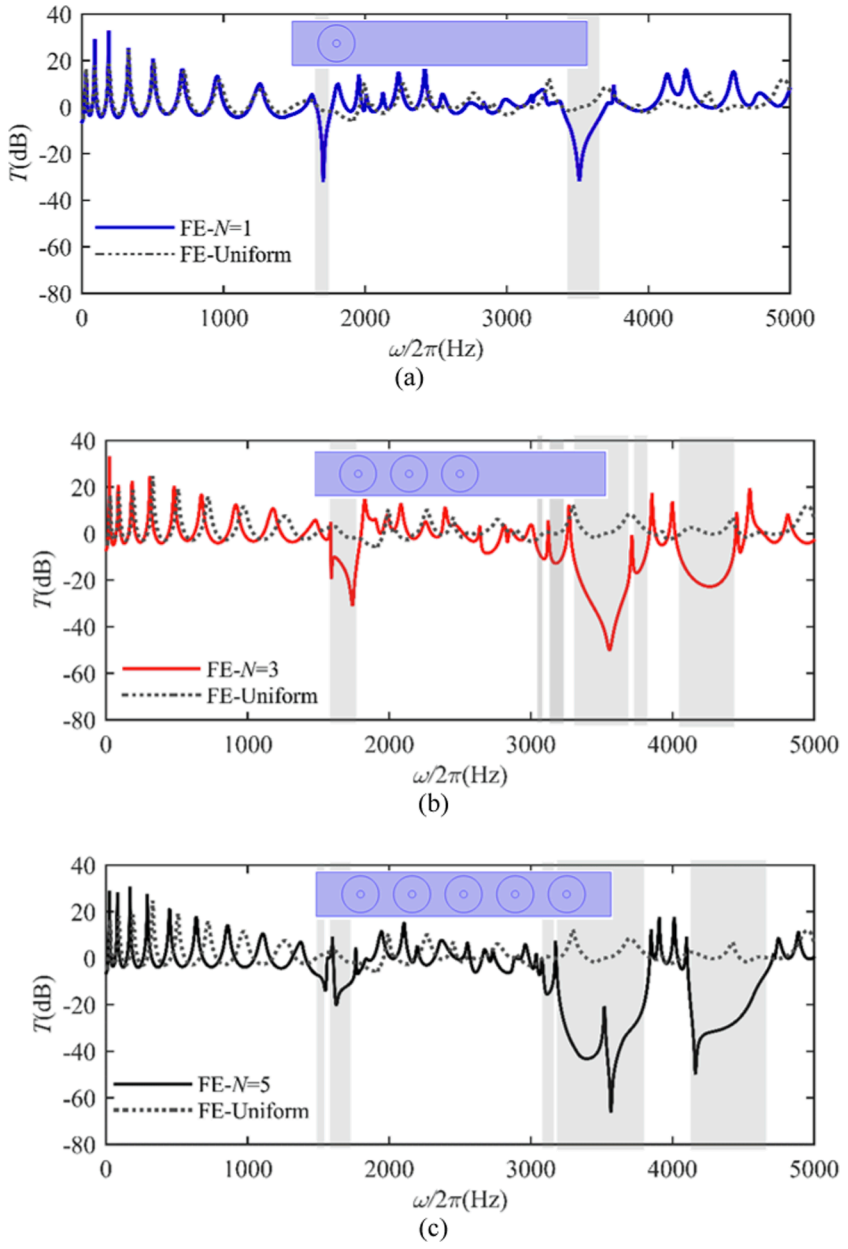

Fig. 6. Vibration transmission ratio calculated by the averaged response at driving and receiving sides for referenced plate strip and ABH-plates with (a) $N = 1$, (b) $N = 3$, and (c) $N = 5$.

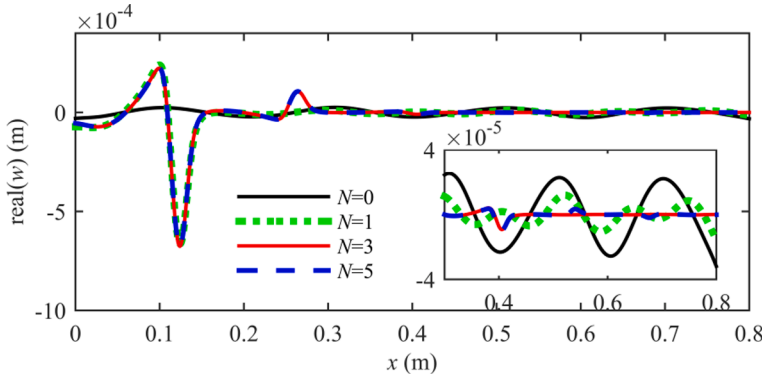

Fig. 7. Displacement along the centerline for the referenced plate strip and ABH-plate at 3550 Hz.

ABHs increases, but the effect is weakened around 1700 Hz.

The displacement distribution of the four plate strips ($N = 0$, 1, 3, 5) along the centerline at 3550 Hz is shown in Fig. 7 to evaluate the effect of ABH indentations on vibration attenuation. According the displacement distribution, it can be concluded that the vibration energy is almost uniformly distributed in the entire uniform plate, but it is concentrated in the ABH indentations in three ABH-plates so that there is less energy in the uniform area. It can be clearly seen that less energy is transmitted to the receiving end as the number of ABH indentation increases. The attenuation of vibration transmission is obviously due to the effect of local structural resonance induced by ABHs. The so-called local structural resonance refers to cases where vibration is much stronger in some local areas of the structure than others. This is different from the locally resonant behavior widely used in phononic crystals, induced by local oscillators coupled with host structure.

4. Attenuation mechanism and discussions

Considering the standing wave form, a finite-size plate strip embedded with multiple 2D ABHs exhibits attenuation bands with low vibration transmission in the length direction of the strip. It is important to investigate the mechanism of the attenuation band phenomenon from the modal analysis perspective. First of all, it is necessary to consider the influence of the cut-off frequencies of some high-order modes in the plate strip due to its relatively narrow width compared with its length. The dispersion curves of the uniform plate strip (a plate strip with a width of 0.12 m, thickness of 5.18 mm and infinite length) is shown in Fig. 8 to illustrate the types of wave modes. As shown in the figure, there are four types of elastic waves: longitudinal (labeled by L), torsional (labeled by T) and bending with respect to y (labeled by BZ because the displacement is in z-direction) and bending with respect to z axis (labeled by BY because the displacement is in y-direction) in the infinite plate strip. Only the BZ waves (BZ0 and BZ1) need to be considered since ABH impose its effects only on flexural wave, which is the focal point of concern here. The fundamental wave mode, BZ0, can propagate at any frequency. The cut-off frequency of the first-order mode, BZ1, is about 2 kHz. Therefore, the vibration modes of the strip are formed by only one wave mode, BZ0, below 2 kHz, and by two wave modes, BZ0 and BZ1, between 2 kHz and 5 kHz, which is the maximum frequency considered in this study.

Although the first-order bending mode has a cut-off frequency within the considered frequency range, there are no attenuation bands in the uniform plate strip. Hence, we would argue that the attenuation bands are not related to the cut-off phenomenon of the

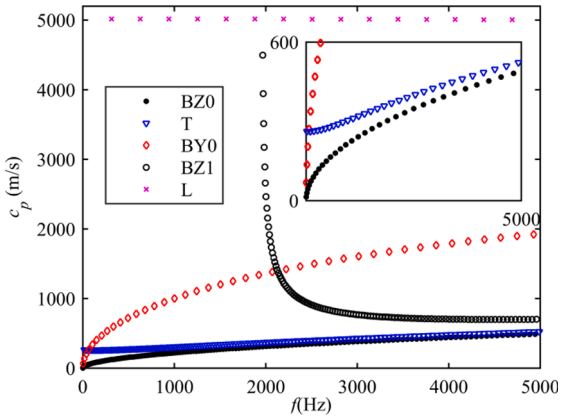

Fig. 8. Dispersion curves for uniform plate strip: phase velocity VS frequency.

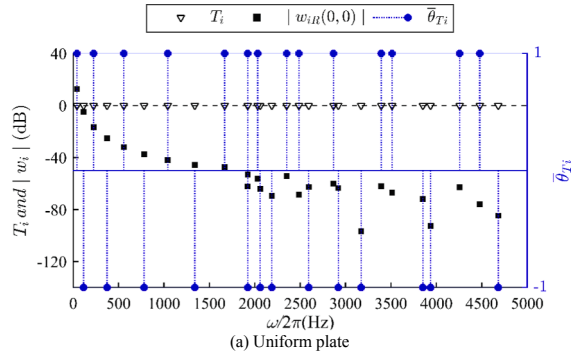

(a) Uniform plate

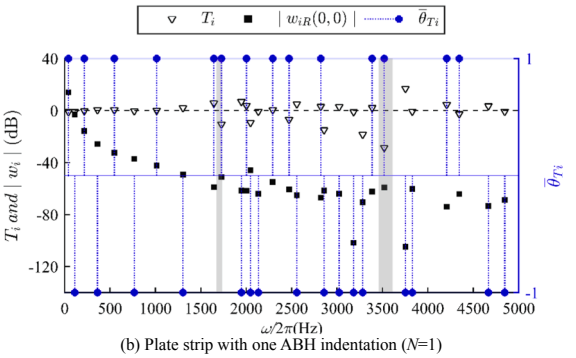

(b) Plate strip with one ABH indentation (N=1)

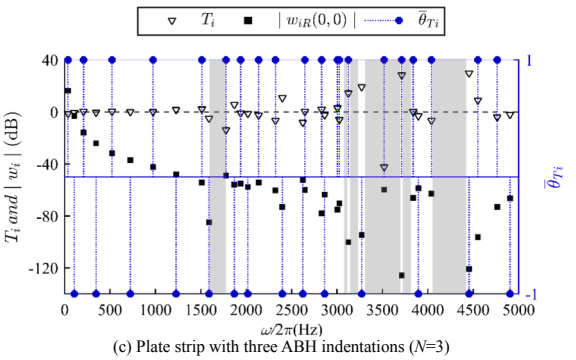

(c) Plate strip with three ABH indentations (N=3)

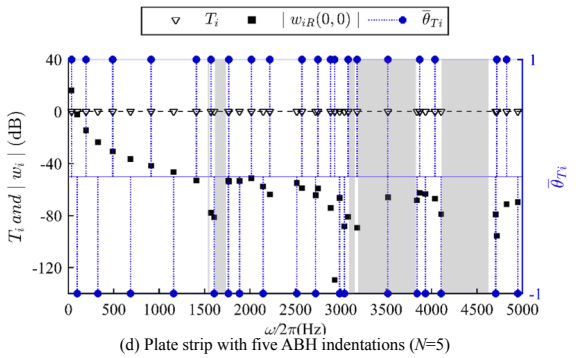

(d) Plate strip with five ABH indentations (N=5)

Fig. 9. The displacement amplitude at the excitation point, modal transmission ratio and phase difference between displacements on the excitation and receiving sides for all modes below 5000 Hz.

high-order modes, but they are ABH-specific characteristics.

In this section, modal analysis for the whole plate strip is therefore used to understand the mechanism of attenuation band formation in ABH-plate. It should be pointed that only the flexural displacement w of the ABH-plates is considered due to the fact that the ABH structure is only effective for flexural waves. The vibration of a plate can be expressed as the superposition of modal vibrations using modal coordinates. Under harmonic excitation $F = F_0 e^{j\omega t}$ (j is the imaginary unit) at position (0, 0), the complex amplitude of flexural displacement response $\overline{w}$ at any point on structure can be expressed as:

$$\overline{w}(x,y) = \sum_{i=1}^{n} \overline{w}_i(x,y) = \sum_{i=1}^{n} q_{i0}\phi_{iz}(x,y) = \sum_{i=1}^{n} |q_{i0}|\phi_{iz}(x,y)e^{-j\theta_{wi}} \tag{5}$$

where ϕ_{iz} is the ith modal function corresponding to the lateral displacement of the plates, $\overline{w}_i$ is the complex amplitude of the ith modal response, q_{i0} is the complex amplitude of modal coordinates and θ_{wi} is the phase. In a structure with the proportional damping defined by the complex modulus in Eq. (3), the complex amplitude q_{i0} can be expressed as:

$$q_{i0} = \frac{\phi_{iz}(0,0)F_0}{\omega_i^2(1-\lambda_i^2 + j2\zeta_i\lambda_i)} \tag{6}$$

where $\lambda_i = \omega/\omega_i$,$\omega_i$is the natural frequency andζ_i denotes the modal damping ratio. There exists the relationship $\eta = 2\zeta_i$ between the damping ratio ζ_i and the loss factor η defined in Eq. (3) for small values of damping [30]. Because no additional damping material is bonded to the structures, the modal loss factor of the structure is the same as the loss factor of the material, η.

Although the average displacements on the excitation side and receiving side have been used in the definition of the transmission ratio in Eq. (4), to reduce the influence of measurement noise in the experiments, the displacments at (0, 0) and (L, 0) are used in the analysis of the tranasmission band formation for convenience, instead of the average displacements on the excitation side and receiving side. According to Eqs. (5) and (6), the input and output displacements are approximately expressed as:

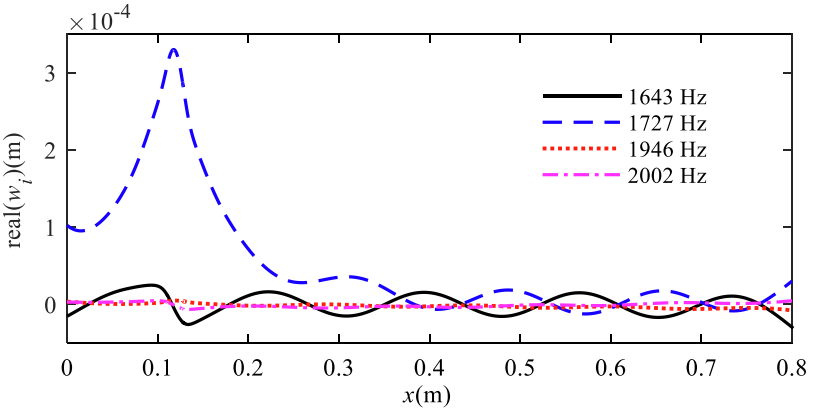

(a) Modal displacement of the 9th, 10th, 11th and 12th modes at 1703 Hz

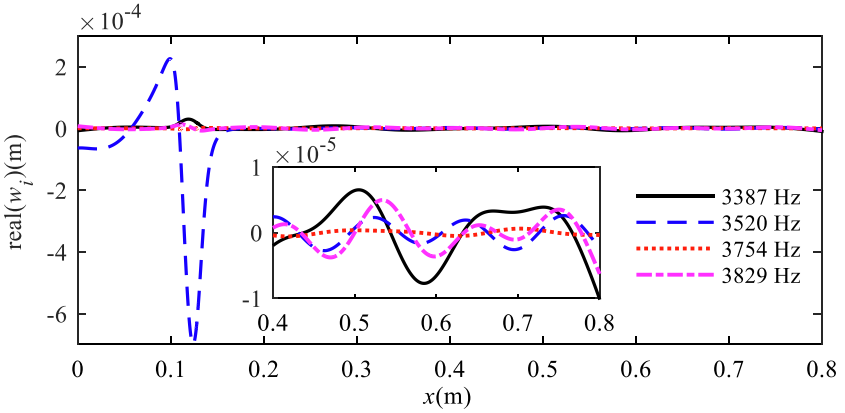

(b) Modal displacement of the 23th, 24th, 25th and 26th modes at 3550 Hz

Fig. 10. The displacement distribution of the selected mode along the centerline for $N = 1$.

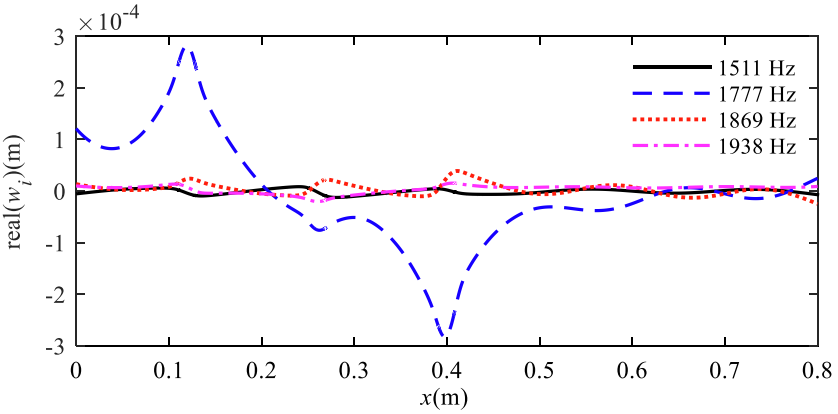

(a) Modal displacement of the 9th, 10th, 11th and 12th modes at 1750 Hz

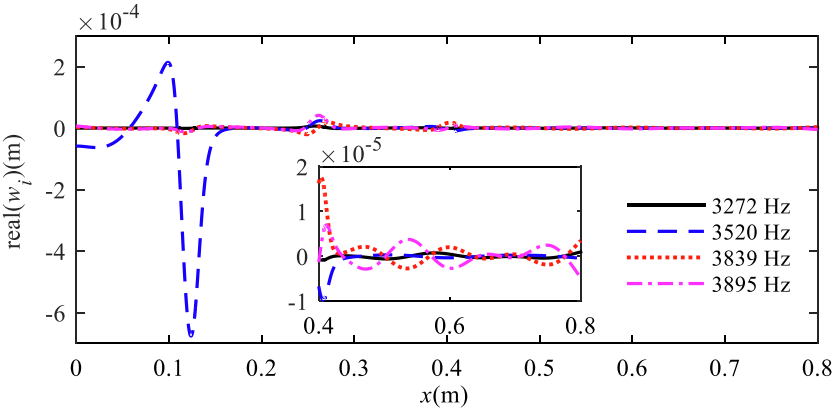

(b) Modal displacement of the 23th, 24th, 25th and 26th modes at 3550 Hz

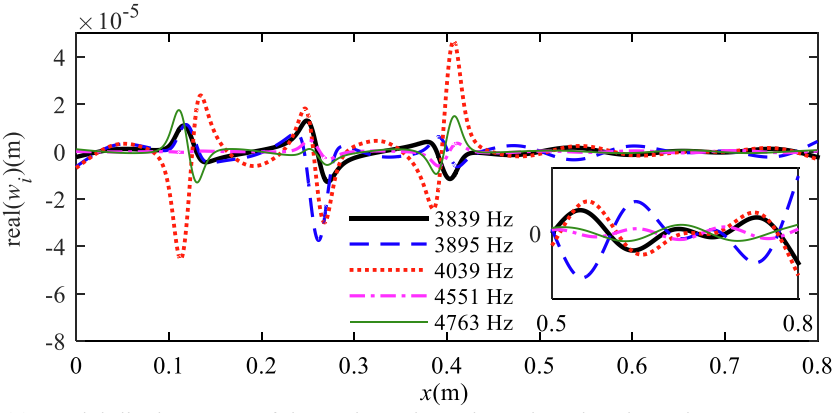

(c) Modal displacement of the 28th, 29th, 30th, 32th and 33th modes at 4244 Hz

Fig. 11. The displacement distribution of the selected mode along the centerline for $N = 3$.

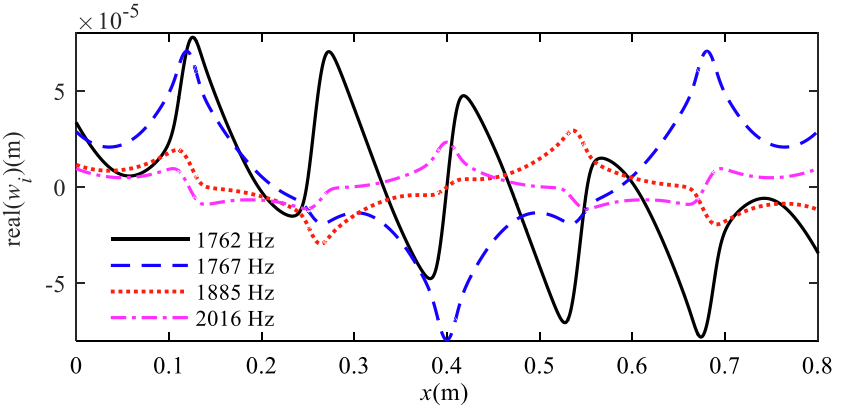

(a) Modal displacement of the 12th, 13th, 14th and 15th modes at 1703 Hz

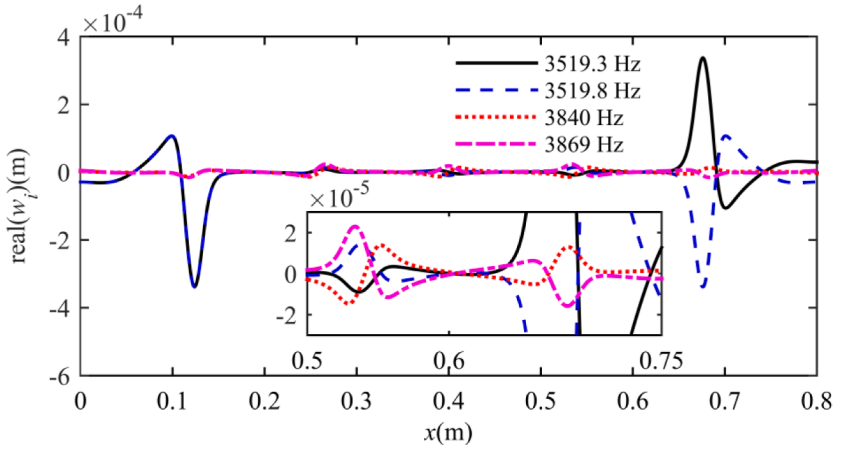

(b) Modal displacement of the 28th, 29th, 30th and 31th modes at 3550 Hz

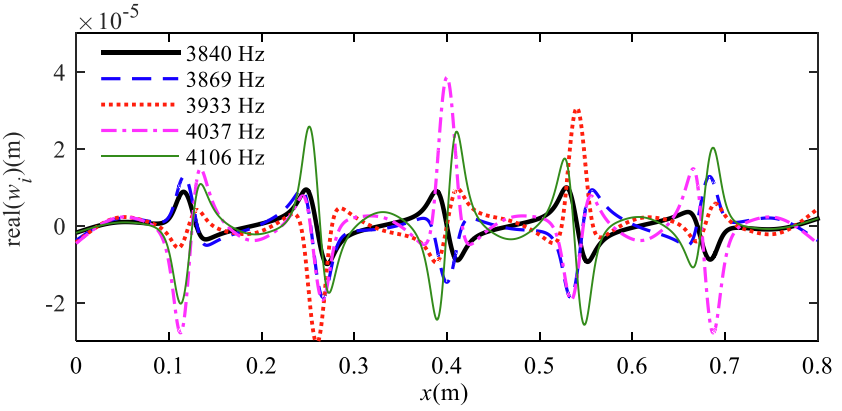

(c) Modal displacement of the 30th, 31th, 32th, 33th and 34th modes at 4230 Hz

Fig. 12. The displacement distribution of the selected mode along the centerline for $N = 5$.

$$\overline{w}_{in} \approx \overline{w}(0,0) = \sum_{i=1}^{n} \frac{\phi_{iz}^2(0,0)F_0 e^{-j\theta_{wi}}}{\omega_i^2|1-\lambda_i^2+j2\zeta_i\lambda_i|}, \overline{w}_{out} \approx \overline{w}(L,0) = \sum_{i=1}^{n} \frac{\phi_{iz}(0,0)\phi_{iz}(L,0)F_0 e^{-j\theta_{wi}}}{\omega_i^2|1-\lambda_i^2+j2\zeta_i\lambda_i|} \tag{7}$$

For convenience of analysis, the following three parameters are defined:

$$T_i = 20log\frac{\left|\overline{w}_i(L,0)\right|}{\left|\overline{w}_i(0,0)\right|} = 20log\frac{|\phi_{iz}(L,0)|}{|\phi_{iz}(0,0)|}, \overline{\theta}_{Ti} = sgn\left(\frac{\phi_{iz}(L,0)}{\phi_{iz}(0,0)}\right),$$

$$w_{iR}(0,0) = \overline{w}_i(0,0)\Big|_{\omega=\omega_i} \tag{8}$$

Obviously, T_i is the transmission ratio of the ith mode, $\overline{\theta}_{Ti}$ is a parameter to show that the phase of vibration at the two points when the plate vibrates in this mode ($\overline{\theta}_{Ti}=1$ for the same phase and $\overline{\theta}_{Ti}=-1$ for the opposite phase) and $w_{iR}(0,0)$ is the value of $w_i(0,0)$ at its resonance frequency. Using $w_{iR}(0,0)$ the input and output displacements can further be expressed as:

$$\overline{w}_{in} \approx \sum_{i=1}^{n} K(\lambda_i)|w_{iR}(0,0)|, \overline{w}_{out} \approx \sum_{i=1}^{n} K(\lambda_i)|w_{iR}(0,0)|\frac{|\phi_{iz}(L,0)|}{|\phi_{iz}(0,0)|}\overline{\theta}_{Ti} \tag{9}$$

in which

$$K(\lambda_i) = \frac{2\zeta_i e^{-j\theta_{wi}}}{|1-\lambda_i^2+j2\zeta_i\lambda_i|}, \theta_{wi}(\lambda_i) = -arctan\left(\frac{2\zeta_i\lambda}{1-\lambda_i^2}\right) \tag{10}$$

According to Eqs. (4), (8) and (9), the transmision ratio depends $K(\lambda_i)$, $|w_{iR}(0,0)|$, T_i and $\overline{\theta}_{Ti}$ of all modes. However, the absolute value of the first frequency-dependent term, $|K(\lambda_i)|$, becomes very small and its phase is approximately 0 or π when λ_i is slightly different from one because the damping ratio is very small ($\zeta = 0.0005$). For example, $|K(0.95)| = 0.0103$, $|K(1.05)| = 0.0098$, $\theta_{wi}(0.95) = 0.0031\pi$ and $\theta_{wi}(1.05) = 0.9967\pi$. When λ_i is far away from 1, the structural response can hardly be excited. Hence, at a considered ω, only a few modes satisfying $\lambda_i = \omega/\omega_i \approx 1$ will dominante $\overline{w}_{in}$ and $\overline{w}_{out}$ and need to be taken into consideration. The value of $|w_{iR}(0,0)|$, T_i and $\overline{\theta}_{Ti}$ of all the modes below 5000 Hz of the four plate strips with $N = 0$, 1, 3 and 5 are shown in Fig. 9, in which the areas marked with grey stripes are bands with over −10 dB attenuation. Obviously, formation of an attenuation band is induced by the change of $w_{iR}(0,0)$, T_i and $\overline{\theta}_{Ti}$ of some modes, which in turn is induced by change of vibration characteristics due to existance of ABH indentations. Hence, further examination of the relationship among the attenuation bands, the value of $w_{iR}(0,0)$, T_i and $\overline{\theta}_{Ti}$, and the vibration characteristics is necessary.

Due to the symmetry of the uniform plate, $T_i = 0$ for all modes as shown in Fig. 9(a). Because $\frac{|\phi_{iz}(L,0)|}{|\phi_{iz}(0,0)|} = 1$, the only difference between $\overline{w}_{in}$ and $\overline{w}_{out}$ in Eq. (9) is the influence of $\overline{\theta}_{Ti}$ in $\overline{w}_{out}$. Opposite signs of $\overline{\theta}_{Ti}$ for the neigboring modes may induce cancellation of modal displacements in $\overline{w}_{out}$ at some frequencies, but no attenuation bands are formed in the uniform plate. Fig. 9(b) shows that two narrow attenuations bands, from 1685 Hz to 1729 Hz and from 3454 Hz to 3602 Hz respectively, are formed in the plate strip with one ABH indentation. Significant changes in $|w_{iR}(0,0)|$ and $T_i$can also be observed. The small transmission ratio of 10th mode at 1727 Hz (T_{10}=−10.62 dB) is certainly an important factor for the formation of the attenuation band, but there may exist other factors because T_{10} is only slightly smaller than the −10 dB threshold and the resonance frequency of 9th (1643 Hz) is very close to the 10th mode. The distribution of displacement of the four modes near the band at 1703 Hz is shown in Fig. 10(a). Obviously, the 10th mode has small transmission ratio due to strong local structural resonance induced by the only one ABH. $w_9(L,0)$ and $w_{10}(L,0)$ have comparable magnitudes but opposite phases, and the small value of $\overline{w}_{out}$ is due to effective cancellation between $w_9(L,0)$ and $w_{10}(L,0)$. The displacement $\overline{w}_{in}$ is relatively large because $w_9(0,0)$ and $w_{10}(0,0)$ cannot cancel each other sufficiently. Because the influence of the 11th mode at 1946 and 12th mode at 2002 Hz is relatively small, a small transmission ratio is induced inside the attenuation band. However, since T_{10} is only slightly smaller than the −10 dB, the influence of the 11th and 12th modes becomes significant as the frequency increases slightly and the influence of the 9th mode becomes significant as the frequency decreases slightly. As a result, the attenuation band is very narrow. From Fig. 9(b) it is obvious that the attenuation band from 3454 Hz to 3602 Hz is due to small transmission ratio of 24th mode at 3520 Hz ($T_{24} = -28.52$ dB). This band is relatively wide because T_{24} is much smaller than the −10 dB threshold. The displacement distribution of the four modes at 3550 Hz in and near the band is shown in Fig. 10(b). The 24th mode has very strong local structural resonance and it is dominant in the formation of attenuation band.

As shown in Fig. 9(c), there are three wide attenuation bands and three narrow ones in the ABH-plate with three ABH indentations. Obviously, the wide attenuation band from 1591 Hz to 1777 Hz is due to the synthetic effect of small transmission ratio of the 11th mode ($T_{11} = -13.85$ dB) at 1777 Hz and weak excitation of the 10th mode at 1590 Hz (-84.94 dB). The band is not extended to a higher frequency due to the strong influence of the 12th mode at 1869 Hz. The distribution of four modal displacements at 1750 Hz shown in Fig. 11(a) also support this. It is also clear that the small transmission ratio of the 11th mode can be attributed to the strong local vibration in two of the three ABH areas. The wide attenuation band from 3303 Hz to 3706 Hz is due to the small transmission ratio of the 26th mode ($T_{26} = -42.39$ dB). The band is wider than that in the ABH-plate with only one indentation because T_{26} in this ABH plate is smaller than T_{24} in the previous plate. Although the 27th mode is weakly excited, it has large transmission ratio ($T_{27} = 28.38$ dB) so that it splits a larger attenuation band generated by the 26th mode into two. The distribution of four modal displacements at

3550 Hz is shown in Fig. 11(b). It is also obvious that strong local structural resonance plays an important role in the formation of attenuation bands. A new wide attenuation band appears from 4056 Hz to 4427 Hz. The displacement of the 31th mode is not shown in the figure because its vibration amplitude is too weak. Because there is no mode inside the band, the transmission ratio is determined by the displacements of the modes neighboring the band. The small transmission ratio is due to the effective cancellation of the displacements of these modes on the receiving side, as shown in Fig. 11(c).

In the ABH-plate with five indentations, there are three wide attenuation bands and two narrow ones. Because it is also symmetrical, the modal transmission ratios of all the modes are 0, similar to the uniform plate. Hence, the only mechanism for formation of attenuation bands is the effective cancellation of displacement of neighboring modes on the receiving side. The displacement distribution of the four neighboring modes at 1703 Hz for the band from 1613 Hz to 1735 Hz is shown in Fig. 12(a). The displacements of the 10th and 11th modes are not illustrated because they weakly excited, as shown in Fig. 9(d). Obviously, the small transmission ratio is due to the fact that the displacements of the four modes accumulate on the exciting side, but cancel one another on the receiving side. Inside the attenuation band from 3189 Hz to 3827 Hz, there are two modes with very close natural frequencies of 3519.25 Hz and 3519.77 Hz, respectively. They have the same value of $w_{iR}(0,0)$, but opposite values of $\overline{\theta}_{Ti}$, so that their displacements at the receiving side can always cancel each other. The displacement distribution of the 28th, 29th, 30th and 31th modes is shown in Fig. 12(b). The formation of the band from 4114 Hz to 4622 Hz is the same as that in the ABH-plate with three indentations because there is no resonance mode inside the band. The displacement distribution of the mode 30th, 31th, 32th, 33th and 34th modes at 4230 Hz is shown in Fig. 12(c). Compared with Fig. 12(b) and (c), the cancellation of displacement in Fig. 12(a) is not perfect due to the weakly local structural resonance induced by ABH cells. It explains why the attenuation for ABH-plate with five indentations is weakened around 1700 Hz, when compared with the case $N = 1$ dominated by the strong local vibration with only one ABH.

From the above results, it can be concluded that there are two types of mechanism in the formation of attenuation bands in ABH-plates: low modal transmission in assymmetrical structures and modal displacement cancellation on the receiving side in both assymmetrical and symmetrical structures. Weak excitation of some modes may enhance the formation of attenuation bands. Most importantly, local structural resonance induced by ABH cells plays an important role in modal transmission reduction, modal displacement cancellation and weak excitation of some modes. Hence, attenuation bands are the special features of ABH structures. Since local structural resonance begins to appear at the frequency of about 1700 Hz, the first attenuation band is generated around this frequency. The fact that the local structural resonance induced by ABH cells plays an important role in the formation of attenuation bands also explains why they appear in the frequencies much lower than the cut-on frequency. It is also obvious that the attenuation bands are not the result of damping effects. The above analysis indicates that lightly damped structure is benificial for the formation of attenuation bands. It cannot be excluded that the boundary conditions would influence the locations of the attenuation bands. However, the general phenomena reported, as well as underlying physical process revealed, are not limited by the type of boundary conditions of the structure.

5. Conclusions

In this paper, a finite plate strip embedded with multiple 2D ABHs without additional damping material is proposed for vibration transmission attenuation. As compared with existing 1D ABH beams, 2D ABHs offers better mechanical properties in term of structural stiffness and strength, more conducive to practical engineering applications. Both the experimental and numerical results show a finite-size plate strip with multiple ABHs exhibits attenuation bands with low vibration transmission below the cut-on frequency, while the width of the attenuation band widens and new attenuation band appears as the number of ABHs increases. The underlying mechanism of attenuation band formation in finite-size ABH plates, which is different from that of the band gap behavior in an infinite lattice of ABHs, is explored based on modal theory. Modal transmission, modal excitation and modal displacement cancellation are used to explain the cause of the attenuation band formation. The local structural resonance induced by ABH cells, which is beneficial for modal transmission reduction, modal displacement cancellation and weak excitation of some modes, is the main factor for the formation of attenuation bands. Two types of mechanisms are clarified for the formation of attenuation bands: low modal transmission in asymmetrical structures and modal displacement cancellation on the receiving side in both asymmetrical and symmetrical structures. The first attenuation band is generated around the first local structural resonance frequency, which provides useful guidance for the future design of low frequency attenuation band. The vibration attenuation phenomenon reveals a new ABH-specific feature enriching the existing knowledge on ABH structures with complex wave paths.

The rich dynamics within ABH areas and the mutual-interactions between ABH cells greatly impact on the attenuation band formation, thus pointing at the possibility of changing the local structural resonance induced by ABHs to tune the attenuation bands. As a possible future work, through extending the present investigation to a full 2D configuration, issues like the variable spatial placements and characteristic parameters of 2D ABHs could be addressed.

CRediT authorship contribution statement

Hongli Ji: Conceptualization, Investigation. **Bing Han:** Investigation, Data curation, Writing - original draft. **Li Cheng:** Methodology. **Daniel J. Inman:** Formal analysis, Validation. **Jinhao Qiu:** Methodology, Project administrative, Supervision.

Declaration of Competing Interest

The authors declare that they have no known competing financial interests or personal relationships that could have appeared to influence the work reported in this paper.

Acknowledgements

This research was supported by the National Natural Science Foundation of China (No. 11532006 & 51775267), the Outstanding Youth Science Foundation of China (No. 52022039), the Research Grants Council of Hong Kong Special Administrative Region, China (PolyU 152023/20E), the Natural Science Foundation of Jiangsu Province (BK20181286), the Equipment Pre-research Foundation (No. 80910010102) and a Project Funded by the Priority Academic Program Development of Jiangsu Higher Education Institutions.

References

[1] V.V. Krylov, New type of vibration dampers utilising the effect of acoustic "black holes", Acta Acust. United Acust. 90 (2004) 830–837.
[2] V.V. Krylov, F.J.B.S. Tilman, Acoustic "black holes" for flexural waves as effective vibration dampers, J. Sound Vib. 274 (2004) 605–619, https://doi.org/10.1016/j.jsv.2003.05.010.
[3] E.P. Bowyer, D.J. O'Boy, V.V. Krylov, F. Gautier, Experimental investigation of damping flexural vibrations in plates containing tapered indentations of power-law profile, Appl. Acoust. 74 (2013) 553–560, https://doi.org/10.1016/j.apacoust.2012.10.004.
[4] L. Zhao, S.C. Conlon, F. Semperlotti, An experimental study of vibration based energy harvesting in dynamically tailored structures with embedded acoustic black holes, Smart Mater. Struct. 24 (2015) 65039, https://doi.org/10.1088/0964-1726/24/6/065039.
[5] E.P. Bowyer, V.V. Krylov, Experimental investigation of damping flexural vibrations in glass fibre composite plates containing one- and two-dimensional acoustic black holes, Compos. Struct. 107 (2014) 406–415, https://doi.org/10.1016/j.compstruct.2013.08.011.
[6] H. Zhu, F. Semperlotti, Improving the performance of structure-embedded acoustic lenses via gradient-index local inhomogeneities, Int. J. Smart Nano Mater. 6 (2015) 1–13, https://doi.org/10.1080/19475411.2015.1009192.
[7] E.P. Bowyer, V.V. Krylov, Damping of flexural vibrations in turbofan blades using the acoustic black hole effect, Appl. Acoust. 76 (2014) 359–365, https://doi.org/10.1016/j.apacoust.2013.09.009.
[8] J. Deng, L. Zheng, P. Zeng, Y. Zuo, O. Guasch, Passive constrained viscoelastic layers to improve the efficiency of truncated acoustic black holes in beams, Mech. Syst. Signal Process. 118 (2019) 461–476, https://doi.org/10.1016/j.ymssp.2018.08.053.
[9] V.B. Georgiev, J. Cuenca, F. Gautier, L. Simon, V.V. Krylov, Damping of structural vibrations in beams and elliptical plates using the acoustic black hole effect, J. Sound Vib. 330 (2011) 2497–2508, https://doi.org/10.1016/j.jsv.2010.12.001.
[10] L. Tang, L. Cheng, H. Ji, J. Qiu, Characterization of acoustic black hole effect using a one-dimensional fully-coupled and wavelet-decomposed semi-analytical model, J. Sound Vib. 374 (2016) 172–184, https://doi.org/10.1016/j.jsv.2016.03.031.
[11] H. Ji, J. Luo, J. Qiu, L. Cheng, Investigations on flexural wave propagation and attenuation in a modified one-dimensional acoustic black hole using a laser excitation technique, Mech. Syst. Signal Process. 104 (2018) 19–35, https://doi.org/10.1016/j.ymssp.2017.10.036.
[12] L. Ma, L. Cheng, Sound radiation and transonic boundaries of a plate with an acoustic black hole, J. Acoust. Soc. Am. 145 (2019) 164–172, https://doi.org/10.1121/1.5081680.
[13] V. Denis, F. Gautier, A. Pelat, J. Poittevin, Measurement and modelling of the reflection coefficient of an Acoustic Black Hole termination, J. Sound Vib. 349 (2015) 67–79, https://doi.org/10.1016/j.jsv.2015.03.043.
[14] Y. Wang, J. Du, L. Cheng, Power flow and structural intensity analyses of Acoustic Black Hole beams, Mech. Syst. Signal Process. 131 (2019) 538–553, https://doi.org/10.1016/j.ymssp.2019.06.004.
[15] L. Tang, L. Cheng, Broadband locally resonant band gaps in periodic beam structures with embedded acoustic black holes, J. Appl. Phys. 121 (2017), 194901, https://doi.org/10.1063/1.4983459.
[16] S.C. Conlon, J.B. Fahnline, F. Semperlotti, Numerical analysis of the vibroacoustic properties of plates with embedded grids of acoustic black holes, J. Acoust. Soc. Am. 137 (2015) 447–457, https://doi.org/10.1121/1.4904501.
[17] P.A. Feurtado, S.C. Conlon, An experimental investigation of acoustic black hole dynamics at low, mid, and high frequencies, J. Vib. Acoust. Trans. ASME. 138 (2016) 1–6, https://doi.org/10.1115/1.4033894.
[18] P.A. Feurtado, S.C. Conlon, Wavenumber transform analysis for acoustic black hole design, J. Acoust. Soc. Am. 140 (2016) 718–727, https://doi.org/10.1121/1.4959023.
[19] E.P. Bowyer, V.V. Krylov, Experimental study of sound radiation by plates containing circular indentations of power-law profile, Appl. Acoust. 88 (2015) 30–37, https://doi.org/10.1016/j.apacoust.2014.07.014.
[20] L. Zhao, Low-frequency vibration reduction using a sandwich plate with periodically embedded acoustic black holes, J. Sound Vib. 441 (2019) 165–171, https://doi.org/10.1016/j.jsv.2018.10.046.
[21] L. Tang, L. Cheng, Periodic plates with tunneled Acoustic-Black-Holes for directional band gap generation, Mech. Syst. Signal Process. 133 (2019), 106257, https://doi.org/10.1016/j.ymssp.2019.106257.
[22] L. Tang, L. Cheng, Ultrawide band gaps in beams with double-leaf acoustic black hole indentations, J. Acoust. Soc. Am. 142 (2017) 2802–2807, https://doi.org/10.1121/1.5009582.
[23] N. Gao, Z. Wei, H. Hou, A.O. Krushynska, Design and experimental investigation of V-folded beams with acoustic black hole indentations, J. Acoust. Soc. Am. 145 (2019) EL79–EL83. https://doi.org/10.1121/1.5088027.
[24] N. Gao, Z. Wei, R. Zhang, H. Hou, Low-frequency elastic wave attenuation in a composite acoustic black hole beam, Appl. Acoust. 154 (2019) 68–76, https://doi.org/10.1016/j.apacoust.2019.04.029.
[25] J. Deng, O. Guasch, L. Maxit, L. Zheng, Reduction of Bloch-Floquet bending waves via annular acoustic black holes in periodically supported cylindrical shell structures, Appl. Acoust. 169 (2020), 107424, https://doi.org/10.1016/j.apacoust.2020.107424.
[26] T. Zhou, L. Tang, H. Ji, J. Qiu, L. Cheng, Dynamic and static properties of double-layered compound acoustic black hole structures, Int. J. Appl. Mech. 9 (2017) 1750074, https://doi.org/10.1142/S1758825117500740.
[27] W. Huang, H. Ji, J. Qiu, L. Cheng, Wave energy focalization in a plate with imperfect two-dimensional acoustic black hole indentation, J. Vib. Acoust. Trans. ASME. 138 (2016) 1–12, https://doi.org/10.1115/1.4034080.
[28] COMSOL, Comsol Multiphysics Reference Manual (Version 4.3b), (2013).
[29] P.G. Dylejko, N.J. Kessissoglou, Y. Tso, C.J. Norwood, Optimisation of a resonance changer to minimise the vibration transmission in marine vessels, J. Sound Vib. 300 (2007) 101–116, https://doi.org/10.1016/j.jsv.2006.07.039.
[30] S. Singiresu, Rao, Mechanical vibrations, fifth ed., Prentice Hall, 2011.